Forces in Optical Near-fields

Lukas Novotny

1 Introduction

As early as 1619 Johannes Kepler suggested that the mechanical effect of light might be responsible for the deflection of the tail of comets entering our solar system. The classical Maxwell theory showed in 1873 that the radiation field carries with it momentum and that "light pressure" is exerted on illuminated objects. In 1905 Einstein introduced the concept of the photon and showed that energy transfer between light and matter occurs in discrete quanta. Momentum and energy conservation was found to be of great importance in microscopic events. The discrete momentum transfer between photons (X-rays) and other particles (electrons) has been experimentally demonstrated by Compton in 1925 and the recoil momentum transferred from photons on atoms has been observed by Frisch in 1933 [2]. Important studies on the action of photons on neutral atoms were made in the 1970's by Letokhov and other researchers in the former USSR and in the group of Ashkin at the Bell Laboratories, USA. The latter group proposed bending and focusing of atomic beams and trapping of atoms in focused laser beams. Later work by Ashkin and co-workers led to the development of "optical tweezers". These devices allow to optically trap and manipulate macroscopic particles and living cells with typical sizes in the range of $0.1 - 10$ micrometers [3,4]. Milliwatts of laser power produce piconewtons of force. Due to the high field gradients of evanescent waves, strong forces are to be expected in optical near-fields. A recent discussion is given in Ref. [1]

The idea that an object might cool through its interaction with the radiation field was suggested already in 1929 by Pringsheim [5]. However, the first proposal to cool atoms in counter-propagating laser beams was made by Hänsch and Schawlow in 1975 [6]. This proposal was the starting point for a series of exciting experiments which led to the 1997 Nobel prize in physics. The mechanical force in laser trapping and cooling experiments can be understood on a semiclassical basis where the electromagnetic field is treated classically and the particle being trapped as a quantized two-level system [7]. However, the quantum theory of photons is used for the correct interpretation of the results [8]. Furthermore, the photon concept asserts that there are

quanta of energy and momentum transfer between the radiation field and the atom.

2 Theory

The general law for forces in electromagnetic fields is based on the conservation law for linear momentum. We therefore derive this conservation law in the following. Later we will discuss two different limits, the dipolar limit and the limit of the planar interface. For simplicity, we consider Maxwell's equations in vacuum. In this case we have $\mathbf{D} = \varepsilon_o \mathbf{E}$ and $\mathbf{B} = \mu_o \mathbf{H}$. Later we will relax this constraint. The conservation law for linear momentum is entirely a consequence of Maxwell's equations

$$\nabla \times \mathbf{E}(\mathbf{r},t) = -\frac{\partial \mathbf{B}(\mathbf{r},t)}{\partial t} \ , \tag{1}$$

$$\nabla \times \mathbf{B}(\mathbf{r},t) = \frac{1}{c^2}\frac{\partial \mathbf{E}(\mathbf{r},t)}{\partial t} + \mu_o \mathbf{j}(\mathbf{r},t) \ , \tag{2}$$

$$\nabla \cdot \mathbf{E}(\mathbf{r},t) = \frac{1}{\varepsilon_o}\rho(\mathbf{r},t) \ , \tag{3}$$

$$\nabla \cdot \mathbf{B}(\mathbf{r},t) = \mathbf{0} \ , \tag{4}$$

and of the force law

$$\begin{aligned} \mathbf{F}(\mathbf{r},t) &= q\left[\mathbf{E}(\mathbf{r},t) + \mathbf{v}(\mathbf{r},t)\times\mathbf{B}(\mathbf{r},t)\right] \\ &= \int_V \left[\rho(\mathbf{r},t)\mathbf{E}(\mathbf{r},t) + \mathbf{j}(\mathbf{r},t)\times\mathbf{B}(\mathbf{r},t)\right] dV \ . \end{aligned} \tag{5}$$

The first expression applies to a single charge q moving with velocity $\mathbf{v}$ and the second expression to a distribution of charges and currents satisfying the charge conservation law

$$\nabla \cdot \mathbf{j}(\mathbf{r},t) + \frac{\partial \rho(\mathbf{r},t)}{\partial t} = 0 \ , \tag{6}$$

which is a direct consequence of Maxwell's equations. The force law connects the electromagnetic world with the mechanical one. The two terms in the first expression are basically definitions of the electric and magnetic field.

If we operate on Maxwell's first equation by $\times\varepsilon_o\mathbf{E}$, on the second equation by $\times\mu_o\mathbf{H}$, and then add the two resulting equations we obtain

$$\varepsilon_o(\nabla\times\mathbf{E})\times\mathbf{E}+\mu_o(\nabla\times\mathbf{H})\times\mathbf{H} = \mathbf{j}\times\mathbf{B}-\frac{1}{c^2}[\frac{\partial\mathbf{H}}{\partial t}\times\mathbf{E}]+\frac{1}{c^2}[\frac{\partial\mathbf{E}}{\partial t}\times\mathbf{H}] \ . \tag{7}$$

We have omitted the arguments $(\mathbf{r},t)$ for the different fields and we used $\varepsilon_o\mu_o = 1/c^2$. The last two expressions in Eq. 7 can be combined to $(1/c^2)\, d/dt\, [\mathbf{E}\times\mathbf{H}]$. For the first expression in Eq. 7 we can write

$$\varepsilon_o(\nabla\times\mathbf{E})\times\mathbf{E} \;=\; \tag{8}$$

$$\varepsilon_o\begin{bmatrix}\partial/\partial x\,(E_x^2-E^2/2)+\partial/\partial y(E_xE_y) & +\partial/\partial z(E_xE_z)\\ \partial/\partial x\,(E_xE_y) & +\partial/\partial y(E_y^2-E^2/2)+\partial/\partial z(E_yE_z)\\ \partial/\partial x\,(E_xE_z) & +\partial/\partial y(E_yE_z) & +\partial/\partial z(E_z^2-E^2/2)\end{bmatrix} - \varepsilon_o\,\mathbf{E}\,\nabla\cdot\mathbf{E}$$

$$=\;\nabla\cdot[\varepsilon_o\mathbf{E}\mathbf{E}\;-\;(\varepsilon_o/2)E^2\,\mathsf{I}]-\rho\mathbf{E}\;.$$

where equation 3 has been used in the last step. The notation $\mathbf{E}\mathbf{E}$ denotes the outer product, $E^2=E_x^2+E_y^2+E_z^2$ is the electric field strength, and I denotes the unit tensor. A similar expression can be derived for $\mu_o(\nabla\times\mathbf{H})\times\mathbf{H}$. Using these two expressions in Eq. 7 we obtain

$$\nabla\cdot[\varepsilon_o\mathbf{E}\mathbf{E}-\mu_o\mathbf{H}\mathbf{H}-\frac{1}{2}\,(\varepsilon_oE^2+\mu_oH^2)\,\mathsf{I}] \;=\; \frac{d}{dt}\frac{1}{c^2}[\mathbf{E}\times\mathbf{H}]+\rho\,\mathbf{E}\;+\;\mathbf{j}\times\mathbf{B}\;. \tag{9}$$

The expression in brackets on the left hand side is called Maxwell's stress tensor in vacuum, usually denoted as T. In cartesian components it reads as

$$\mathsf{T} \;=\; [\varepsilon_o\mathbf{E}\mathbf{E}-\mu_o\mathbf{H}\mathbf{H}\;-\;\frac{1}{2}\,(\varepsilon_oE^2+\mu_oH^2)\,\mathsf{I}] \;= \tag{10}$$

$$\begin{bmatrix}\varepsilon_o(E_x^2-E^2/2)\;+\;\mu_o(H_x^2-H^2/2) & \varepsilon_oE_xE_y\;+\;\mu_oH_xH_y & \varepsilon_oE_xE_z\;+\;\mu_oH_xH_z\\ \varepsilon_oE_xE_y\;+\;\mu_oH_xH_y & \varepsilon_o(E_y^2-E^2/2)\;+\;\mu_o(H_y^2-H^2/2) & \varepsilon_oE_yE_z\;+\;\mu_oH_yH_z\\ \varepsilon_oE_xE_z\;+\;\mu_oH_xH_z & \varepsilon_oE_yE_z\;+\;\mu_oH_yH_z & \varepsilon_o(E_z^2-E^2/2)\;+\;\mu_o(H_z^2-H^2/2)\end{bmatrix}.$$

After integration of Eq. 9 over an arbitrary volume V which contains all sources ρ and $\mathbf{j}$ we obtain

$$\int_V\nabla\cdot\mathsf{T}\,dV \;=\; \frac{d}{dt}\frac{1}{c^2}\int_V[\mathbf{E}\times\mathbf{H}]\,dV\;+\;\int_V[\rho\,\mathbf{E}\;+\;\mathbf{j}\times\mathbf{B}]\,dV\;. \tag{11}$$

The last term is recognized as the mechanical force (c.f. Eq. 5). The volume integral on the left can be transformed to a surface integral using Gauss' integration law

$$\int_V\nabla\cdot\mathsf{T}\,dV \;=\; \int_{\partial V}\mathsf{T}\cdot\mathbf{n}\,da\;. \tag{12}$$

∂V denotes the surface of V, $\mathbf{n}$ the unit vector perpendicular to the surface, and da an infinitesimal surface element. We then finally arrive at the conservation law for linear momentum

$$\int_{\partial V}\mathsf{T}(\mathbf{r},t)\cdot\mathbf{n}(\mathbf{r})\,da \;=\; \frac{d}{dt}\left[\mathbf{G}_{field}(\mathbf{r},t)\;+\;\mathbf{G}_{mech}(\mathbf{r},t)\right]\;. \tag{13}$$

where $\mathbf{G}_{mech}$ and $\mathbf{G}_{field}$ denote the mechanical momentum and the field momentum, respectively. In Eq. 13 we have used Newton's expression of the mechanical force $\mathbf{F} = d/dt\,\mathbf{G}_{mech}$ and the definition of the field momentum

$$\mathbf{G}_{field} \;=\; \frac{1}{c^2}\int_V [\mathbf{E}\times\mathbf{H}]\,dV\;. \tag{14}$$

This is the momentum carried by the electromagnetic field within the volume V. It is created by the dynamic terms in Maxwell's curl equations, i.e. by the terms containing the time derivative. The field momentum is zero when it is averaged over one oscillation period and the average force becomes

$$\langle\mathbf{F}\rangle \;=\; \int_{\partial V}\langle\mathsf{T}(\mathbf{r},t)\rangle\cdot\mathbf{n}(\mathbf{r})\;da\;, \tag{15}$$

with $\langle..\rangle$ denoting the time average. Equation 15 is of general validity. It allows to calculate the mechanical force acting on an arbitrary body within the closed surface ∂V. The force is entirely determined by the electric and magnetic fields on the surface ∂V. It is interesting to note that no material properties enter the expression for the force; the entire information is contained in the electromagnetic field. The only material constraint is that the body is rigid. If the body deforms when it is subject to an electromagnetic field we have to include electro- and magnetorestrictive forces. Since the enclosing surface is arbitrary the same results are obtained whether the fields are evaluated at the surface of the body or in the farfield. It is important to note that the fields used to calculate the force are the self-consistent fields of the problem which means that they are a superposition of the incident and the scattered fields. Therefore, prior to calculating the force, one has to solve

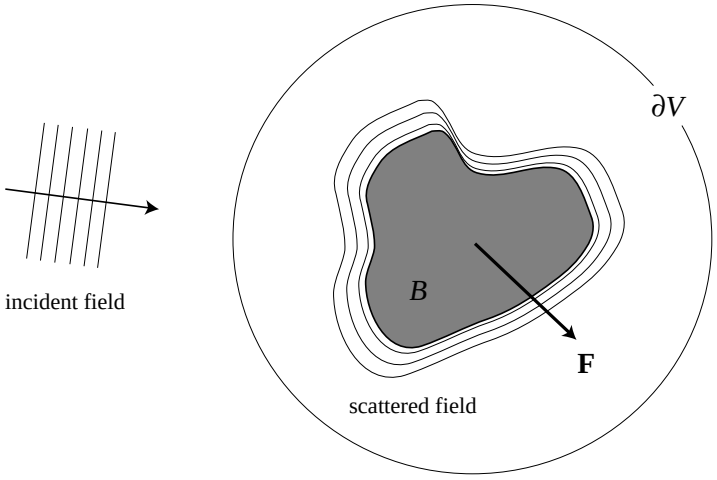

Fig. 1. The mechanical force $\mathbf{F}$ acting on the object B is entirely determined by the electric and magnetic fields at an arbitrary surface ∂V enclosing B.

for the electromagnetic fields. If the object B is surrounded by a medium which can accurately enough be represented by the dielectric constant ε and magnetic susceptibility μ the mechanical force can be calculated in the same way if we replace Maxwell's stress tensor Eq. 10 by

$$\mathsf{T} \;=\; [\varepsilon_o \varepsilon \mathbf{EE} \,-\, \mu_o \mu \mathbf{HH} \,-\, \frac{1}{2}\,(\varepsilon_o \varepsilon E^2 \,+\, \mu_o \mu H^2)\mathsf{I}] \,. \tag{16}$$

2.1 Radiation Pressure

In this subsection we consider the radiation pressure on a medium with an infinitely extended planar interface as shown in Fig. 2. The medium is irradiated by a monochromatic plane wave at normal incidence to the interface. Depending on the material properties of the medium, part of the incident field is reflected at the interface. Introducing the complex reflection coefficient R, the electric field outside the medium can be written as the superposition of two counter propagating plane waves

$$\mathbf{E}(\mathbf{r},t) \;=\; E_o \,\mathrm{Re}\Big\{[e^{ikz} \,+\, R\, e^{-ikz}]\, e^{-i\omega t}\Big\}\,\mathbf{n}_x \,. \tag{17}$$

Using Maxwell's curl equation 1 we find for the magnetic field

$$\mathbf{H}(\mathbf{r},t) \;=\; \sqrt{\varepsilon_o/\mu_o}\; E_o \,\mathrm{Re}\Big\{[e^{ikz} \,-\, R\, e^{-ikz}]\, e^{-i\omega t}\Big\}\,\mathbf{n}_y \,. \tag{18}$$

To calculate the radiation pressure P we integrate Maxwell's stress tensor on an infinite planar surface A parallel to the interface as shown in Fig. 2. The radiation pressure can be calculated by using Eq. 15 as

$$P\,\mathbf{n}_z \;=\; \frac{1}{A}\int_A \langle \mathsf{T}(\mathbf{r},t)\rangle \cdot \mathbf{n}_z \; da \,. \tag{19}$$

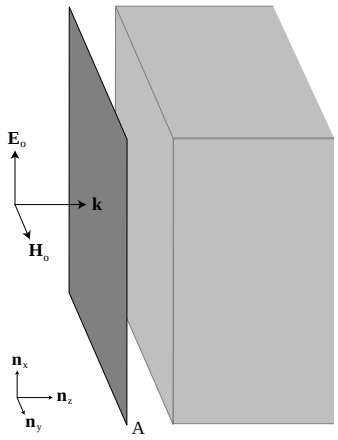

Fig. 2. Configuration used to derive the radiation pressure.

We do not need to consider a closed surface ∂V since we are interested in the pressure exerted on the interface of the medium and not in the mechanical force acting on the medium. Using the fields of Eqs. 17 and 18 we find that the first two terms in Maxwell's stress tensor Eq. 10 give no contribution to the radiation pressure. The third term yields

$$\langle \mathsf{T}(\mathbf{r},t)\rangle \cdot \mathbf{n}_z \;=\; -\frac{1}{2}\langle \varepsilon_o E^2 + \mu_o H^2\rangle \,\mathbf{n}_z \;=\; \frac{\varepsilon_o}{2}\,E_o^2\,[1+|R|^2]\,\mathbf{n}_z\;. \tag{20}$$

Using the definition of the intensity of a plane wave $I_o = (\varepsilon_o/2)c\,E_o^2$, c being the vacuum speed of light, we can express the radiation pressure as

$$P \;=\; \frac{I_o}{c}\,[1\,+\,|R|^2]\;. \tag{21}$$

For a perfectly absorbing medium we have $R = 0$, whereas for a perfectly reflecting medium $R = 1$. Therefore, the radiation pressure on a perfectly reflecting medium is twice as high as for a perfectly absorbing medium.

2.2 Dipole Approximation

Let us consider two oppositely charged particles with masses m_1, m_2, separated by a tiny distance $|\mathbf{s}|$, and illuminated by an arbitrary electromagnetic field $\mathbf{E}$, $\mathbf{B}$, as shown in Fig. 3. In the nonrelativistic limit, the equation of motion for each particle follows from Eq. 5 by setting $\mathbf{F}$ equal to $m_1\ddot{\mathbf{r}}_1$ and $m_2\ddot{\mathbf{r}}_2$, respectively. The dots denote differentiation with respect to time. Since the particles are bound to each other we have to consider their binding energy U. Including this contribution, the equation of motion for the two particles reads as

$$m_1\,\ddot{\mathbf{r}}_1 = \;\; q\,[\mathbf{E}(\mathbf{r}_1,t) \;+\; \dot{\mathbf{r}}_1\times\mathbf{B}(\mathbf{r}_1,t)] \;-\; \nabla U(\mathbf{r}_1,t)\;, \tag{22}$$

$$m_2\,\ddot{\mathbf{r}}_2 = -q\,[\mathbf{E}(\mathbf{r}_2,t) \;+\; \dot{\mathbf{r}}_2\times\mathbf{B}(\mathbf{r}_2,t)] \;+\; \nabla U(\mathbf{r}_2,t)\;. \tag{23}$$

The two particles constitute a two body problem which is most conveniently solved by introducing the center of mass coordinate

$$\mathbf{r} \;=\; \frac{m_1}{m_1+m_2}\,\mathbf{r}_1 \;+\; \frac{m_2}{m_1+m_2}\,\mathbf{r}_2\;. \tag{24}$$

Expressing the problem in terms of $\mathbf{r}$ allows us to separate the internal motion of the two particles from the center of mass motion. The electric field at the position of the two particles can be represented by a Taylor expansion as [9]

$$\mathbf{E}(\mathbf{r}_1) = \sum_{n=0}^{\infty}\Big[(\mathbf{r}_1-\mathbf{r})\cdot\nabla\Big]^n\,\mathbf{E}(\mathbf{r}) \;=\; \mathbf{E}(\mathbf{r}) + (\mathbf{r}_1-\mathbf{r})\cdot\nabla\mathbf{E}(\mathbf{r}) \;+\; \ldots\;, \tag{25}$$

$$\mathbf{E}(\mathbf{r}_2) = \sum_{n=0}^{\infty}\Big[(\mathbf{r}-\mathbf{r}_2)\cdot\nabla\Big]^n\,\mathbf{E}(\mathbf{r}) \;=\; \mathbf{E}(\mathbf{r}) - (\mathbf{r}_2-\mathbf{r})\cdot\nabla\mathbf{E}(\mathbf{r}) \;+\; \ldots\;.$$

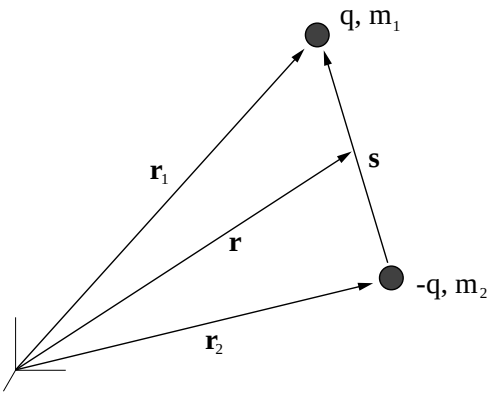

Fig. 3. Graphical representation of the symbols used to derive the mechanical force in the dipolar limit. $\mathbf{r}$ denotes the center of mass coordinate. The two particles are bound to each other by the potential U.

A similar expansion can be found for $\mathbf{B}(\mathbf{r}_1)$ and $\mathbf{B}(\mathbf{r}_2)$. For $|\mathbf{s}| \ll \lambda$, λ being the wavelength of the radiation field, the expansions can be truncated after the second term (dipole approximation). A strait forward calculation using equations 22-25 and the definition of the dipole moment

$$\mathbf{p} \;=\; q\,\mathbf{s}\;, \tag{26}$$

where $\mathbf{s} = \mathbf{r}_1 - \mathbf{r}_2$ leads to [8]

$$\begin{aligned}\mathbf{F} &= (m_1 + m_2)\,\ddot{\mathbf{r}} \\ &= (\mathbf{p}\cdot\nabla)\,\mathbf{E} \;+\; \dot{\mathbf{p}} \times \mathbf{B} \;+\; \ddot{\mathbf{r}} \times (\mathbf{p}\cdot\nabla)\,\mathbf{B}\;.\end{aligned} \tag{27}$$

Here, we have omitted the arguments $(\mathbf{r}, t)$ for clarity. The brackets in $(\mathbf{p}\cdot\nabla)\,\mathbf{E}$ indicate that the inner product $\mathbf{p}\cdot\nabla = (p_x, p_y, p_z)\cdot(\partial/\partial x, \partial/\partial y, \partial/\partial z)$ has to be evaluated prior to operating on $\mathbf{E}$. Equation 27 is the central equation of this subsection. It renders the mechanical force exerted by the electromagnetic field on the two particles represented by the dipole moment $\mathbf{p}$. The force consists of three terms: the first originates from the inhomogeneous electric field, the second is the familiar Lorentz force, and the third is due to movement in the inhomogeneous magnetic field. Usually, the third term is much smaller than the other two terms and it will be omitted in the following discussion. It is interesting to note that the fields appearing in Eq. 27 correspond to the exciting field. It is assumed that the system represented by the dipole does not change the fields. This is different to the general formalism based on Maxwell's stress tensor where the self-consistent fields are considered.

A quantized two-level system such as an atom with transitions restricted to two states is well described by a dipole. The same is true for a macroscopic particle with dimensions much smaller than the wavelength of the

illuminating light (Rayleigh particle). For simplicity we will refer to the system represented by the dipole as particle. Let us consider a particle irradiated by an arbitrary monochromatic electromagnetic wave with angular frequency ω. In this case the fields can be written as

$$\begin{aligned}\mathbf{E}(\mathbf{r},t) &= \mathrm{Re}\{\mathbf{E}(\mathbf{r})\, e^{-i\omega t}\} \\ \mathbf{B}(\mathbf{r},t) &= \mathrm{Re}\{\mathbf{B}(\mathbf{r})\, e^{-i\omega t}\}\ ,\end{aligned} \tag{28}$$

and the dipole moment as

$$\mathbf{p}(t) \;=\; \mathrm{Re}\{\mathbf{p}\, e^{-i\omega t}\}\ . \tag{29}$$

The fields and dipole moment can be represented by their complex amplitudes $\mathbf{E}(\mathbf{r}), \mathbf{B}(\mathbf{r}), \mathbf{p}$. In what follows we will refer by $\mathbf{E}, \mathbf{B}, \mathbf{p}$ to the complex amplitudes. We assume that the particle has no static dipole moment. In this case, to first order, the induced dipole moment is proportional to the electric field at the particle's position $\mathbf{r} = \mathbf{r}_o$

$$\mathbf{p} \;=\; \alpha(\omega)\, \mathbf{E}(\mathbf{r}_o)\ . \tag{30}$$

α denotes the polarizability of the particle. Its form depends on the nature of the particle (two-level system, Rayleigh particle, ..). In the time-average Eq. 27 reads as

$$\langle \mathbf{F} \rangle \;=\; \frac{1}{2}\mathrm{Re}\left\{(\mathbf{p}^*\cdot\nabla)\,\mathbf{E} \;-\; i\omega\,(\mathbf{p}^*\times\mathbf{B})\right\}\ , \tag{31}$$

where we have dropped the third term as discussed before. If we replace the dipole moment by its expression in Eq. 30 and split the polarizability into its real part α' and imaginary part α'', we find after some rearrangements

$$\langle \mathbf{F} \rangle = (\alpha'/2)\,\nabla E^2 \;+\; \omega\,\alpha''\,(\mathbf{E}\times\mathbf{B}) \tag{32}$$

$$= -\nabla V_{pot} \;+\; (\alpha''\omega/\varepsilon_o)\;\mathbf{g}_{field}\ , \tag{33}$$

where $\mathbf{g}_{field}$ denotes the density of the field momentum (c.f. Eq. 14) and V_{pot} the potential energy of the induced dipole moment. We find that two different terms determine the mechanical force: the first is denoted as dipole force (or gradient force) and the second one as scattering force. The dipole force originates from field inhomogeneities. It is proportional to the dispersive part (real part) of the complex polarizability. On the other hand, the scattering force is proportional to the field strength (Poynting vector) and to the dissipative part (imaginary part) of the complex polarizability. The scattering force may also be regarded as a consequence of the momentum delivered by the scattered photons to the particle. For a lossless particle there is no momentum transfer from the radiation field to the particle and the scattering force is zero. Polarizable particles are accelerated by the dipole force towards extrema of the radiation field. Therefore, a tightly focused laser beam can trap a particle in all dimensions at its focus. However, the scattering force

pushes the particle in direction of propagation and if the focus of the trapping laser is not tight enough, the particle might be pushed out of the focus.

In atom manipulation experiments the scattering force is used to cool atoms down to extremely low temperatures thereby bringing them almost to rest. At ambient conditions atoms and molecules move at speeds of about $1000\,m/s$ in random directions. Even at temperatures as low as $-270°C$ the speeds are on the order of $100\,m/s$. Only for temperatures close to absolute zero ($-273°C$) the motion of atoms slows down significantly. The initial idea to slow down the motion of atoms is based on the Doppler effect. It was first proposed by Hänsch and Schawlow in 1975 [6]. Neutral atoms are irradiated by pairs of counter propagating laser beams. If an atom moves against the propagation direction of one of the laser beams the frequency as seen from the atom will shift towards higher frequencies (blue shift) according to the Doppler effect. On the other hand, an atom moving in direction of beam propagation will experience a shift towards lower frequencies (red shift). If the laser frequency is tuned slightly below a resonance transition, an atom will predominantly absorb a photon when it moves against laser beam propagation. The absorption process slows the atom down according to momentum conservation. Once the atom is excited it will eventually reemit its excitation energy by spontaneous emission which is a random process and does not favor any particular direction.

Thus, averaged over many absorption/emission cycles, the atom moving towards the laser will lose velocity and effectively cool. To slow the atom down in all dimensions one requires six laser beams opposed in pairs and arranged in three directions at right angles to each other. Whichever direction the atom tries to move it will be met by photons of the right energy and pushed back into the area where the six laser beams intersect. The movement of the atoms in the intersection region is similar to the movement in a hypothetical viscous medium (optical molasses). It can be calculated that two-level atoms cannot by cooled below a certain temperature, called the Doppler limit [8]. For sodium atoms the limiting temperature is $240\mu K$ corresponding to speeds of $30\,cm/s$. However, it was experimentally found that much lower temperatures could be attained. After surpassing another limit, the so-called recoil limit which states that the speed of an atom should not be less than that imparted by a single photon recoil, temperatures as low as $0.18\,\mu K$ have been generated for helium atoms. Under these conditions the helium atoms move at speeds of only $2\,cm/s$. So far, the atoms are slowed down, but not captured. An optical atom trap is needed to prevent the atoms from falling out of the optical molasses due to gravity. An initial trapping scheme based on the dipole force allowed to grip the atoms at the focal point of a tightly focused beam [10]. Unfortunately, the optical dipole trap was not strong enough for most applications and a new three-dimensional trap based on the scattering force has been developed. This kind of trap is now

called the magneto-optic trap. Its restoring force comes from a combination of oppositely directed circularly polarized laser beams and a weak, varying, inhomogeneous magnetic field with a minimum in the intersection region of the laser beams. The magnetic field strength increases with distance from the trap center and gives rise to a force towards the trap center. For more detailed descriptions on laser cooling and trapping experiments the reader is referred to Refs. [11–13].

In principle, any macroscopic object can be regarded to be composed of individual dipolar subunits. The self-consistent solution for the electric and magnetic fields generated by these dipoles is [14,15]

$$\mathbf{E}(\mathbf{r}) = \mathbf{E}_o(\mathbf{r}) \; + \; \omega^2 \mu_o \sum_{n=1}^{N} \mathsf{G}(\mathbf{r}, \mathbf{r}_n) \cdot \mathbf{p}_n \tag{34}$$

$$\mathbf{H}(\mathbf{r}) = \mathbf{H}_o(\mathbf{r}) \; - \; i\omega \sum_{n=1}^{N} \left[\nabla \times \mathsf{G}(\mathbf{r}, \mathbf{r}_n) \right] \cdot \mathbf{p}_n \qquad \mathbf{r} \neq \mathbf{r}_n \; ,$$

where we used the complex representation of the time-harmonic fields. G denotes the dyadic Green's function, $\mathbf{p}_n$ the electric dipole moment at $\mathbf{r} = \mathbf{r}_n$, and $\mathbf{E}_o$, $\mathbf{H}_o$ the exciting field. The system is assumed to consist of N individual dipoles. To first order, the dipole moment $\mathbf{p}_n$ is

$$\mathbf{p}_n = \alpha(\omega) \, \mathbf{E}(\mathbf{r}_n) \; . \tag{35}$$

Combining equations 34 and 35 we obtain implicit equations for the fields $\mathbf{E}$ and $\mathbf{H}$ which can be solved by matrix inversion techniques. In principle, the mechanical force acting on an arbitrary object made of single dipolar subunits can be determined by using Eq. 33 in combination with Eqs. 34 and 35.

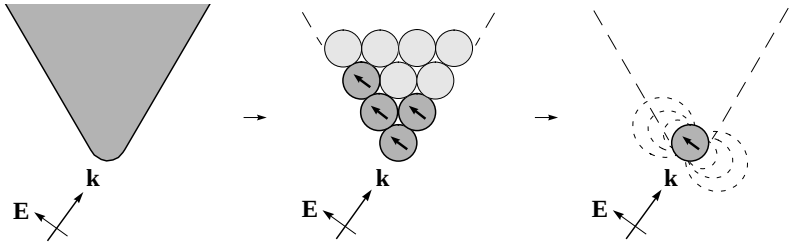

Fig. 4. Illustration of the coupled dipole approach. A macroscopic object is subdivided into individual microscopic dipolar subunits. Each dipole moment can be calculated self-consistently by using the Green's function formalism. In a rough approximation the field in front of a metal tip can be replaced by the field of a single dipole. However, the parameters of the polarizability have to be deduced from a rigorous calculation.

However, if we require that the object does not deform under the influence of the electromagnetic field, the internal forces must cancel and the mechanical force is entirely determined by the fields outside of the object. In this case, the mechanical force can be determined by solving for the fields outside the object and evaluating Maxwell's stress tensor according to Eqs. 10 and 15.

3 Trapping by a Laser Illuminated Metal Tip

As an application of the so forth outlined theory we consider a sharp, laser illuminated gold tip. This configuration has been proposed for the trapping of nanometric particles and biomolecules in aqueous environments [19]. The resulting electric field distribution for this geometry is strongly polarization dependent as shown in Fig. 5. The figure shows the electric field intensity E^2 near the foremost part of the gold tip ($5\,nm$ tip radius) for two different monochromatic plane-wave excitations. The wavelength of the illuminating light is $\lambda = 810\,nm$ (Ti:sapphire laser), which does not match the surface plasmon resonance. The dielectric constants of tip and water were taken to be $\varepsilon = -24.9 + 1.57i$ and $\varepsilon = 1.77$, respectively. In Fig. 5a, a plane-wave is incident from the bottom with the polarization perpendicular to the tip axis,

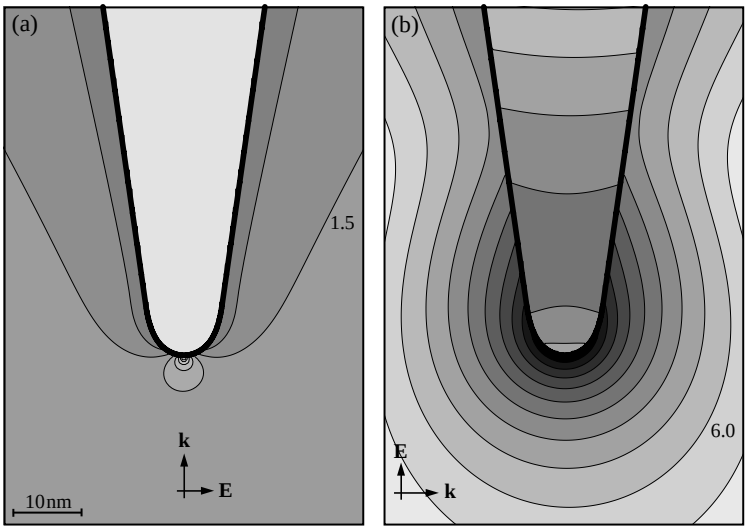

Fig. 5. Near-field of a gold tip in water illuminated by two different monochromatic waves at λ=810nm. Direction and polarization of the incident wave is indicated by the **k** and **E** vectors. The figures show contours of E^2 (factor of 2 between successive lines). The scaling is given by the numbers in the figures (multiples of the exciting field). No enhancement at the tip in (a); enhancement of $\approx$3000 in (b). The field in (b) is almost rotationally symmetric in the vicinity of the tip.

whereas in Fig. 5b the tip is illuminated from the side with the polarization parallel to the tip axis. A striking difference is seen for the two different polarizations: in Fig. 5b, the intensity enhancement at the foremost part of the tip is ≈ 3000 times stronger than the illuminating intensity, whereas no enhancement beneath the tip exists in Fig. 5a. This result suggests that it is crucial to have a large component of the excitation field along the axial direction to obtain a high field enhancement. Calculations of platinum and tungsten tips show lower enhancements, whereas the field beneath a dielectric tip is reduced compared to the excitation field.

Fig. 6 shows the calculated induced surface charge density for the two situations shown in Figs. 5a and 5b. The incident light drives the free electrons in the metal along the direction of polarization. While the charge density is zero inside the metal at any instant of time ($\nabla \cdot \mathbf{E} = 0$), charges accumulate on the surface of the metal. When the incident polarization is perpendicular to the tip axis [Fig. 5a], diametrically opposed points on the tip surface have opposite charges. As a consequence, the foremost end of the tip remains uncharged. On the other hand, when the incident polarization is parallel to the tip axis [Fig. 5b], the induced surface charge density is rotationally symmetric and has the highest amplitude at the end of the tip. In both cases the surface charges form an oscillating standing wave (surface plasmons) with wavelengths shorter than the wavelength of the illuminating light. While the field enhancement has been calculated in the electrostatic limit [18], the pres-

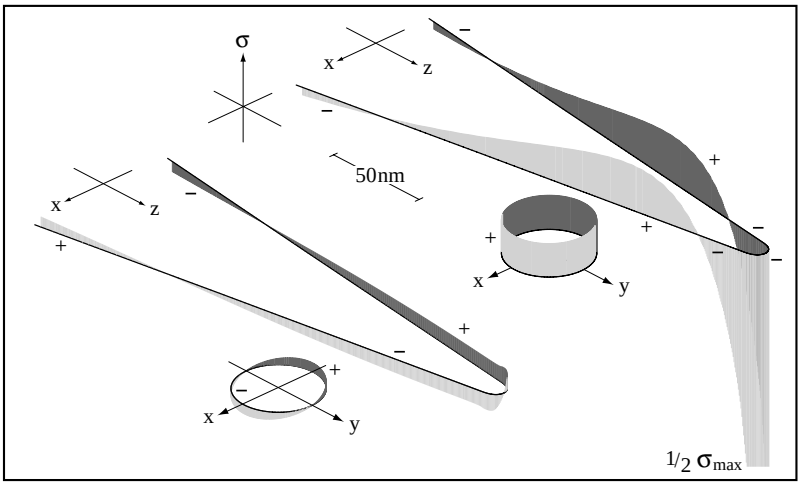

Fig. 6. Induced surface charge density corresponding to Fig. 5a (left) and Fig. 5b (right). The surface charges form a standing wave in each case. In Fig. 5a, the surface charge wave has a node at the end of the tip, whereas in Fig. 5b there is a large surface charge accumulation at the foremost part, responsible for the field enhancement.

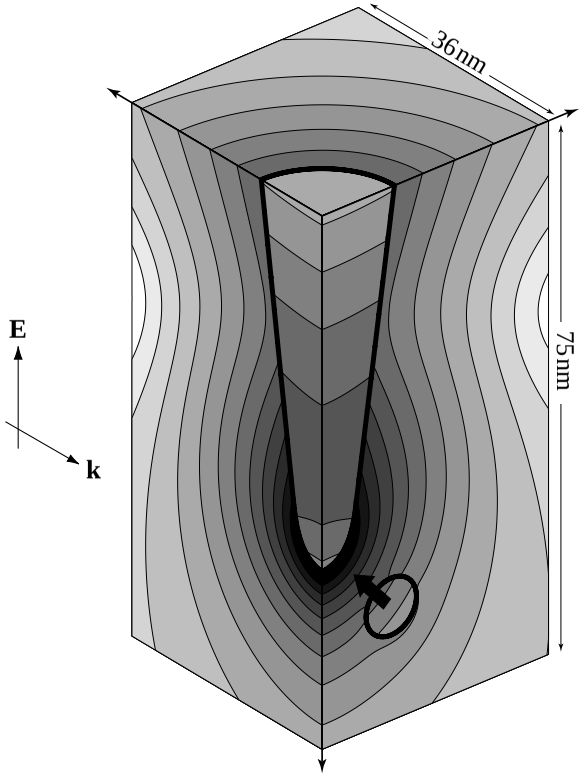

Fig. 7. Perturbation of the near-field by a particle being trapped ($\varepsilon = 2.5$, $10nm$ diameter). The field inside the particle is highly inhomogeneous, requiring rigorous calculation of the trapping force. The arrow indicates the direction of the trapping force. Same scaling as in Fig. 5b.

ence of surface plasmons indicate that it is essential to include retardation in the analysis.

With the field distribution around the tip determined, the gradient force for a Rayleigh particle can be easily calculated as

$$\mathbf{F} = (\alpha/2)\,\nabla E^2\,, \tag{36}$$

where α is the polarizability of the particle. The particle tends to move to the higher intensity region where its induced dipole has lower potential energy. The assumptions inherent in Eq. 36 are that the external field is homogeneous across the particle and that the particle does not alter the field $\mathbf{E}$ in Eq. 36. These assumptions however, do not hold for a nanometric particle close to the tip as shown in Fig. 7. The intensity contours are distorted around a dielectric sphere ($\varepsilon = 2.5$, $10\,nm$ diameter) and the field inside the sphere is

highly inhomogeneous.

Nevertheless, in order to be able to follow the underlying physics without elaborate computations, we will represent both tip and particle by a point dipole. The error of this approximation can then be estimated by comparison with the exact solutions of Ref. [19]. The situation that we are going to analyze is shown in Fig. 8. The sharply pointed metal tip is illuminated by a plane wave at right angle such that the polarization is parallel to the tip axis. The factor f of the enhanced electric field intensity in front of the tip is determined by the material properties, the sharpness and shape of the tip, and the wavelength of the illuminating field [16–18]. We denote the dipoles of tip and particle by $\mathbf{p}_t$ and $\mathbf{p}_p$, respectively. Without loss of generality, the tip dipole is chosen to be located at the origin of the coordinate system. To further simplify the situation, we assume that the coupling between tip and particle can be neglected. In this picture, the incident field $\mathbf{E}_o$, $\mathbf{H}_o$ excites a dipole moment $\mathbf{p}_t$ in the tip and the fields generated by $\mathbf{p}_t$ induce a dipole moment $\mathbf{p}_p$ in the particle. The dielectric constant of particle and environment are $\varepsilon_p(\omega)$ and $\varepsilon_s(\omega)$, respectively. The polarizability of the particle in the nonretarded regime can be calculated as

$$\alpha_p(\omega) \;=\; 3\,\varepsilon_o\,\varepsilon_s(\omega)\,\Delta V_p\,\frac{\varepsilon_p(\omega)-\varepsilon_s(\omega)}{\varepsilon_p(\omega)+2\,\varepsilon_s(\omega)}\;, \tag{37}$$

where ΔV_p is the particle volume.

According to the coupled dipole formalism, any object can be subdivided into dipolar subunits. In a metal, these units have to be chosen so dense

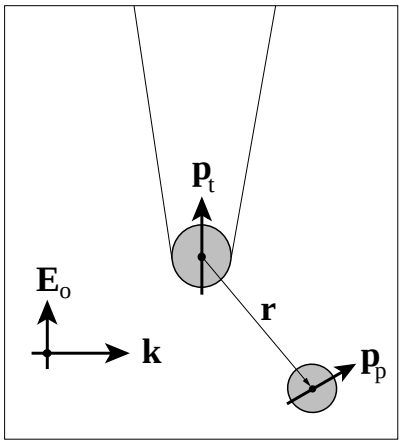

Fig. 8. Trapping of a particle by a laser illuminated metal tip. The tip is illuminated by a plane wave polarized along the tip axis. Both tip and particle are represented by a dipole.

that the field at the tip cannot be attributed to the closest dipole alone. Consequently, the metal tip cannot be approximated by a single polarizable sphere as it is often done for dielectric tips [20]. However, rigorous calculations show that the spatial distribution of the fields close to the metal tip are similar to the field of a vertical dipole. The dipole moment $\mathbf{p}_t$ can be expressed in terms of the computationally determined enhancement factor, f, for the electric field intensity as

$$\mathbf{E}(x=0, y=0, z=a_t) \;=\; \frac{2\;\mathbf{p}_t}{4\pi\,\varepsilon_o\,\varepsilon_s\,a_t^3} \;\equiv\; \sqrt{f}\,\mathbf{E}_o \;, \tag{38}$$

where a_t denotes the tip radius and $(x, y, z) = (0, 0, a_t)$ is the foremost point of the tip. In this equation we have only considered the near-field of the dipole since $k\,a_t \ll 1$. Thus, we find for the tip dipole $\mathbf{p}_t \;=\; 2\pi\,\varepsilon_o\,\varepsilon_s\,a_t^3\sqrt{f}\,\mathbf{E}_o$. To determine the mechanical force on the particle in the vicinity of the tip we have to evaluate Eq. 33. Since we consider tip-particle distances d for which $kd \ll 1$ we can neglect retardation effects and consider quasi-static fields. We can also neglect the scattering force (second term in Eq. 33) because of the small particle size and because there is no radiation pressure associated with the near-fields. In this case we have

$$\langle \mathbf{F} \rangle \;=\; (\alpha_p'/2)\,\nabla E^2(\mathbf{r}) \;. \tag{39}$$

The electric field in this equation corresponds to the field generated by the tip dipole $\mathbf{p}_t$ evaluated at the particle's position $\mathbf{r}$. Its square amplitude reads as

$$E^2(\mathbf{r}) \;=\; \frac{|\mathbf{p}_t|^2}{(4\pi\,\varepsilon_o\,\varepsilon_s)^2}\,\frac{1 \,+\, 3\,(z/r)^2}{r^6} \;, \tag{40}$$

where $r = |\mathbf{r}|$ is the tip-particle distance and $z = \mathbf{r}\cdot\mathbf{n}_z$ is the projection of $\mathbf{r}$ on the tip axis, $\mathbf{n}_z$ being the unit vector along the tip axis. A comparison of the non-retarded fields of a single dipole and the fields of the rigorous solution for the laser illuminated metal tip is shown in Fig. 9. Combining Eqs. 38 - 40 we find for the mechanical trapping force

$$\langle \mathbf{F} \rangle \;=\; -(3/4)\,a_t^6\,f\,E_o^2\,\alpha_p'\,\frac{1}{r^6}\left[\rho\,(1 + 4\,z^2/r^2)\mathbf{n}_\rho \,+\, 4\,z^3/r^2\,\mathbf{n}_z\right] \;, \tag{41}$$

$\mathbf{n}_\rho$ being the unit vector in radial direction perpendicular to the tip axis and $\rho = \mathbf{r}\cdot\mathbf{n}_\rho$. The minus sign indicates that the force is directed towards the tip. We find that $\langle \mathbf{F} \rangle$ is proportional to the enhancement factor f, the intensity of the illuminating light $I_o = 1/2\,\sqrt{\varepsilon_o\,\varepsilon_s/\mu_o}\,E_o^2$, the real part of the particle polarizability α_p', and the sixth power of the tip radius a_t. It has to be kept in mind, that f and a_t are not independent parameters; their relationship can be determined by rigorous calculations only.

In a next step we calculate the trapping potential

$$V_{pot}(\mathbf{r}) \;=\; -\int_{\infty}^{\mathbf{r}} \langle \mathbf{F}(\mathbf{r}') \rangle \, d\mathbf{r}' \;, \tag{42}$$

which corresponds to the potential energy of the particle in the field of the tip dipole. The integration path from $\mathbf{r}$ to ∞ is arbitrary because $\mathbf{F}$ is a conservative vector field. After carrying out the integration we find

$$V_{pot}(\mathbf{r}) \;=\; -a_t^6 \, f \, E_o^2 \, \alpha_p' \, \frac{1 + 3\,z^2/r^2}{8 r^6} \;. \tag{43}$$

The maximum value of V_{pot} is reached exactly in front of the tip ($z = a_t + a_p$). Fig. 10 shows $V_{pot}(\mathbf{r}_p)$ along the tip axis and along a transverse axis immediately in front of the tip. An enhancement factor of $f = 3000$ is assumed and the radii of both tip and particle are chosen as $a_t = a_p = 5nm$. The dielectric constant of particle and environment are $\varepsilon_p = 2.5$ (biomolecule) and $\varepsilon_s = 1.77$ (water), respectively. Since in aqueous environments the trapping forces compete with Brownian motion, the potential in Fig. 10 is normalized with $k_B T$ (k_B = Boltzmann constant, $T = 300K$). Additionally, the curves are scaled with the incident intensity I_o. To have a trapping potential which is just equal to $k_B T$ at room temperature, an intensity of $I_o \approx 100 mW/\mu m^2$ is required. It has to be noticed that the present calculation is a rough approximation. Comparison with the rigorous treatment in Ref. [19] shows that the present results are off by a factor $\approx 2 - 3$. However, the general shape of

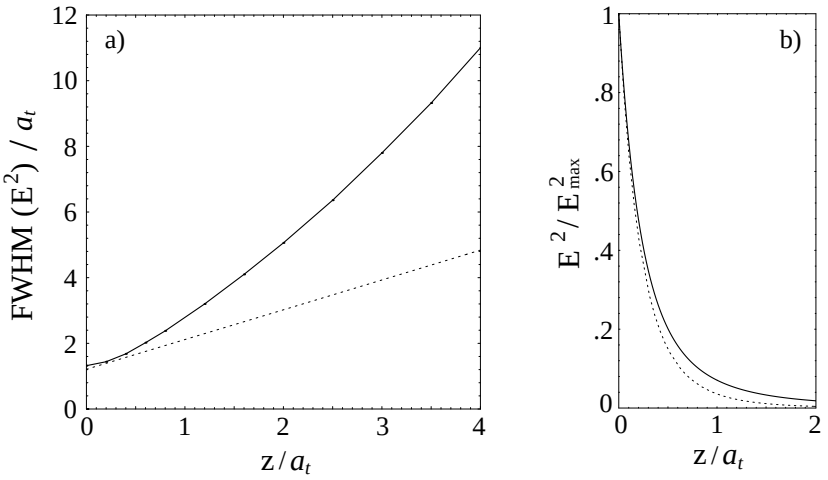

Fig. 9. Comparison of the nonretarded fields of a single dipole (dotted curves) and the rigorous solution for the laser illuminated metal tip (solid curves). Figure a) shows the lateral spread of the field (perpendicular to tip axis) as a function of the distance z from the foremost point of the tip. Figure b) shows the decay of the field along the tip axis. A normalization with the tip radius $a_t = 5nm$ is applied.

the trapping potential is in accordance with Ref. [19].

Let us assume for the following that a sufficient condition for trapping is $V_{pot} > k_B T$. We can then calculate the intensity required to trap a particle of a given size. Using the expression 37 for the particle polarizability and evaluating Eq. 43 at $\mathbf{r} = (a_t + a_p)\mathbf{n}_z$ we find

$$I_o \; > \; \frac{kTc}{4\pi\sqrt{\varepsilon_s}} \, \mathrm{Re}\left\{ \frac{\varepsilon_p + 2\,\varepsilon_s}{\varepsilon_p - \varepsilon_s} \right\} \, \frac{(a_t + a_p)^6}{f\, a_t^6\, a_p^3} \quad . \tag{44}$$

The curve for which the equality holds is shown in Fig. 11. The same parameters are used as above. The minimum in the curve indicates that the incident intensity and the tip radius can be adjusted to selectively trap particles with sizes in a limited range. Too small particles are not trapped because their polarizability is too small. On the other hand, for too big particles the minimum separation between tip and particle $(a_t + a_p)$ becomes too large. For the presently used parameters the optimum particle size is $a_p \approx 5\,nm$. However, since the trapping fields decay slower the larger the tip radius is, it can be expected that for larger tip sizes the optimum particle size becomes larger. As a rule of thumb, the particle size should be in the range of the tip size. Finally, it should be noted that instead of calculating first the trapping force, the potential $V_{pot}(\mathbf{r})$ could have been easier determined by considering the interaction energy of the particle in the dipole approximation. With $\mathbf{E}$ being the field of the tip dipole $\mathbf{p}_t$ it is easy to show that

$$V_{pot}(\mathbf{r}) \; = \; -\mathbf{p}_p \cdot \mathbf{E}(\mathbf{r}) \; = \; -(\alpha_p'/2)\, E^2(\mathbf{r}) \; , \tag{45}$$

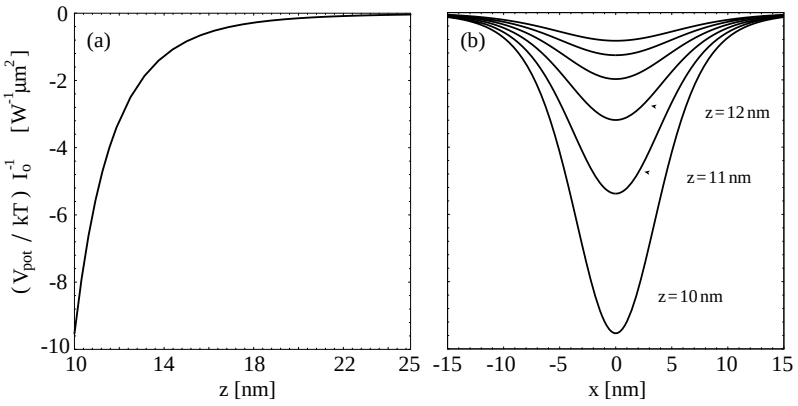

Fig. 10. Trapping potential V_{pot} along the tip axis (a) and along a transverse direction at $z = a_t + a_p$ beneath the tip. An enhancement factor of $f = 3000$ is assumed. The radii of tip and particle are $a_t = a_p = 5\,nm$. The dielectric constant of particle and environment are $\varepsilon_p = 2.5$ (biomolecule) and $\varepsilon_s = 1.77$ (water), respectively. Normalization with $k_B T$ and incident intensity I_o.

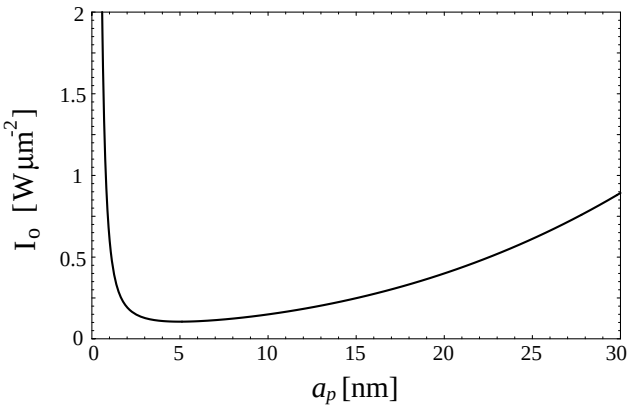

Fig. 11. Minimum trapping intensity I_o as a function of the particle radius a_p. An enhancement factor of $f = 3000$ is assumed and the tip radius is $a_t = 5\,nm$. The dielectric constant of particle and environment are $\varepsilon_p = 2.5$ (biomolecule) and $\varepsilon_s = 1.77$ (water), respectively.

leads to the same result as Eq. 43.

In conclusion, we have outlined a general formalism to calculate the forces on arbitrary objects in electromagnetic fields. The formalism is independent of the material properties of the object being trapped and therefore has general validity. The optical properties of the object enter the formalism indirectly through the solution for the electromagnetic fields. Based on a simple model we have shown that moderate laser powers are needed to trap a nanoparticle at the end of a gold tip in an aqueous environment. Preliminary experimental results have shown that the formation of eddy currents in the aqueous environment do have an effect on the trapping scheme. These eddy currents are generated by laser heating of the metal tip. Although the temperature increase for the required laser powers is small, it is necessary to perform near-field trapping experiments at favorable conditions (air, vacuum). This will lead to a better understanding of the underlying parameters.

References

1. Pohl D. W. (1995) in *Forces in Scanning Probe Methods* of NATO Advanced Study Institute, Series E **286**, edited by H.-J. Güntherodt, D. Anselmetti, and E. Meyer. Kluwer, Dordrecht, 235
2. Frisch R. (1933) Experimenteller Nachweis des Einsteinischen Strahlungsrückstosses. Z. Phys. **86**, 42
3. Ashkin A. (1987) Optical trapping and manipulation of neutral particles using lasers. Proc. Natl. Acad. Sci. USA **94** 4853
4. Svoboda K., Block S. M. (1994) Biological Applications of Optical Forces. Ann. Rev. Biophys. Biomol. Struct. **23**, 247

5. Pringsheim B. (1929) Zwei Bemerkungen über den Unterschied von Lumineszenz- und Temperaturstrahlung. Z. Phys. **57**, 739
6. Hänsch T. W., Schawlow A. L. (1975) Cooling of gases by laser radiation. Opt. Commun. **13**, 68
7. Shimizu Y., Sasada H. (1998) Mechanical force in laser cooling and trapping. Am. J. Phys. **66**, 960
8. Stenholm S. (1986) The semiclassical theory of laser cooling. Rev. Mod. Phys. **58**, 699
9. Arfken G. (1985) Mathematical Methods for Physicists (3rd ed.). Academic Press, New York
10. Chu S., Bjorkholm J. E., Ashkin A., Cable A. (1986) Experimental observation of optically trapped atoms. Phys. Rev. Lett. **57**, 314
11. Cohen-Tannoudji C. N., Phillips W. D. (1990), New mechanisms for laser cooling. Physics Today **10**, 33
12. Chu S. (1992) Laser trapping of neutral particles. Scientific American **2**, 71
13. Lubkin G. B. (1996) Experimenters cool Helium below single-photon recoil limit in three dimensions. Physics Today **1**, 22
14. Martin O. J. F., Dereux A., Girard C., (1994) Iterative scheme for computing exactly the total field propagating in dielectric structures of arbitrary shape. J. Opt. Soc. Am. A **11**, 1073
15. Novotny L., (1997) Allowed and forbidden light in near-field optics. II. Interacting dipolar particles. J. Opt. Soc. Am. A **14**, 105
16. Novotny L., Sanchez E. J., Xie X. S. (1998) Near-field optical imaging using metal tips illuminated by higher-order Hermite-Gaussian beams. Ultramicroscopy **71**, 21
17. Martin O. J. F., Girard C. (1997) Controlling and tuning strong optical field gradients at a local probe microscope tip apex. Appl. Phys. Lett. **70**, 705
18. Denk W., Pohl D. W. (1991) Near-field optics: Microscopy with nanometer-size fields. J. Vac. Sci. and Technol. B **9**, 510
19. Novotny L., Bian R. X., Xie X. S. (1997) Theory of nanometric optical tweezers. Phys. Rev. Lett. **79**, 645
20. Labeke D. V., Barchiesi D., (1993) Theoretical problems in scanning near-field optical microscopy, in *Near Field Optics* (D. W. Pohl and D. Courjon, eds.), vol. 242 of *NATO Advanced Study Institute, Series E.* Dordrecht: Kluwer Academic Publishers, 157